Open Access

SCHOLARENA

Journal of Nanoscience and Nanotechnology Applications

RESEARCH ARTICLE

ISSN: 2577-7920

Investigation of Structural and Electrical Properties of Manganese Doped ZnO Varistors Prepared from Nanopowders

Boumezoued A[1*], Guergouri K[1], Zaabat M[1], Recham D[2] and Barille R[3]

[1]*Laboratory of Active Components and Materials, University Larbi Ben M'hidi of Oum El Bouaghi, Algeria*

[2]*Laboratory of Materials and Structure of Electro mechanic Systems and Their Fiability, University Larbi Ben M'hidi of Oum El Bouaghi, Algeria*

[3]*Moltech Anjou University Angers/Cnrs Umr, Bd Lavoisier Angers Cedex, France*

[*]**Corresponding author:** Boumezoued A, Laboratory of Active Components and Materials, University Larbi Ben M'hidi of Oum El Bouaghi, Algeria, Tel: +213.6.61.30.91.96, E-mail: kamelguergouri@yahoo.com; amal.boum4@gmail.com

Citation: Boumezoued A, Guergouri K, Zaabat M, Recham D, Barille R (2018) Investigation of Structural and Electrical Properties of Manganese Doped ZnO Varistors Prepared from Nanopowders. J Nanosci Nanotechnol 2: 306

Abstract

Non-ohmic properties of pure and doped zinc oxide varistors are widely used to manufacture good devices. These varistors are generally used in electrical or electronic circuits to protect them from voltage surges. In this study, pure and Mn doped ZnO nanopowders have been synthesized by a soft chemistry method, the sol-gel route. The obtained powders after calcination at 500 °C are consolidated and sintered using conventional furnace at 1075 °C for 15 min. The obtained pellets are characterized by: X-ray diffraction, MET. The XRD spectra indicate that pure and Mn doped ZnO powders are solid solution, with an average grain size varying between 36.15 nm to 65.92 nm. The grain size decreases with the increase of Mn concentration except for 5 mol % Mn, where there is an unexpected increase. This is confirmed by MET images. The current-voltage J(E) characteristics show that the breakdown electric field increases with increasing Mn concentration ranging from 1595V/cm to 1901.50V/cm except for the Zn-5% Mn-O varistor, where the non linear coefficient α and breakdown electric field are lower. In general the more the grain size decreases the more the varistor effect and the threshold voltage increase.

Keywords: ZnO; Nanomaterials; Sol-Gel; Nano-powders; Varistors

Introduction

Nanomaterials have received a great interest in last decades due to their many technological applications, very promising in various fields such as sensors, field-emission transistors, ultraviolet photo-detectors, photovoltaic and biomedical system such as DNA sequence detectors [1]. Among these materials, zinc oxide (ZnO) is considered as one of the most important in varistor behavior because of its excellent non-ohmic properties and a high non-linearity coefficient [2,3]. Varistors based on ZnO have been most extensively studied [4,5]. At the same time researchers have made considerable efforts to develop and investigate new properties in this material for protection against over voltages in electrical network or a power supply. Thus, in the literature, there are varistors based on tin dioxide (SnO_2), titanium dioxide (TiO_2), strontium titanate ($SrTiO_3$), barium titanate ($BaTiO_3$), tungsten trioxide (WO_3) and dioxide of cerium (CeO_2) [6-16]. In comparison, varistors based on zinc oxide are more interesting since they present a coefficient of non-linearity α ten times more high. For this reason ZnO became the best choice. To improve the coefficient α and to favor the states of interface, several oxides such as Bi_2O_3, Pr_6O_{11}, SbO_3, CoO or MnO are added to ZnO matrix. ZnO nanopowders are synthesized by various techniques, the most widely used at this time is the sol-gel route, because of its low cost one hand, and the good quality of the varistors made with. The origin of the varistor effect is essentially due to the microstructure in one hand, and to the potential barriers of grain boundaries between two ZnO, in another hand [17-19].

The grain boundaries are therefore responsible for the non-linearity because each one of them constitutes a barrier to the passage of the current. Therefore, the size of grains in a varistor determines the number of grain boundaries that the current will encounter on its way and therefore the threshold voltage of the varistor.

The purpose of this study was therefore the investigation of the effect of manganese on the structural, optical and electrical properties of ZnO varistors.

Details Experimental

Materials and Procedures

Pure and Mn-doped ZnO nanopowders have been synthesized by the soft chemistry sol-gel technique. Zinc acetate dehydrate ($C_4H_6O_4Zn.2H_2O$) (purity>99%, biochem-Chempharma) is used as starting material and an alcoxide: citric acid ($C_6H_8O_7.H_2O$) monohydrate is used to keep particles in suspension, monoethanolamine MEA (C_2H_7NO) and ethylene glycol are used as a stabilizer and solvent, respectively. The dopant source of manganese used is manganese chloride ($MnCl_3$). Then, the obtained solution is stirred at 130 °C for 2h to obtain a homogeneous and transparent solution. Finally and after 24h the solution was calcined at 500 °C for 4h in a furnace.

The obtained powders are characterized by means of several techniques: XRD, using the Cukα (kα = 0.154056 nm) radiation of a BRRUKER AXS, D8 advance X-ray diffract meter, to identify the structure and calculate the grain size, TEM, using an X-Max model transmission electron microscope to identify the morphology and estimate the crystallite size, electrical characteristics J(E), using a high voltage measure unit (KEITHLEY model 237) to calculate the breakdown electric field and non linear coefficient α.

In order to obtain dense varistors with high performance, conventional sintering study was performed. To do that, the obtained powders were pressed into discs of 11mm in diameter and 1.8mm in thickness at a pressure of 2 MPa. Then the pellets were sintered at 1750 °C for 15 min. The size of the final samples was about 10 mm in diameter and 1.6 mm in thickness. Gold contact was deposited on both faces of the pellets of Zn% Mn-O to have ohmic contacts, which are realized by heating at 500 °C for 10 min to remove the organic functions.

Results and Discussion

The XRD patterns of Zn1-xMnxO (0≤x≤7) powders synthesized by sol-gel method are shown in Figure 2. The spectra exhibit peaks of the würtzite structure. It is also shown that two peaks were detected at 29.39° and 33.05° only in Zn5%Mn-O corresponding to Mn_3O_4 phase as identified by Sharma, *et al.*, which reported the presence of secondary phases: $ZnMn_2O_3$ or Mn_3O_4 in the Mn doped ZnO [20].

The average grain sizes were calculated from X-ray line broadening using Scherrer formula (1) [21].

$$D = \frac{0.9\lambda}{\Delta\theta\cos\theta} \quad (1)$$

Where D is the grain size, λ the X-ray wave length (λ=1.5418A°), Δθ the full width at half-maximum (FWHM) and θ the Bragg angle.

Lattice parameters a and c of the samples were calculated using the following equation (2):

$$\frac{1}{d} = \frac{4}{3}\left[\frac{h^2 + hk + k^2}{2}\right] + \frac{l^2}{c} \quad (2)$$

Where a and c are the lattice parameters, d is the interplanar distance and (hkl) are the miller indices

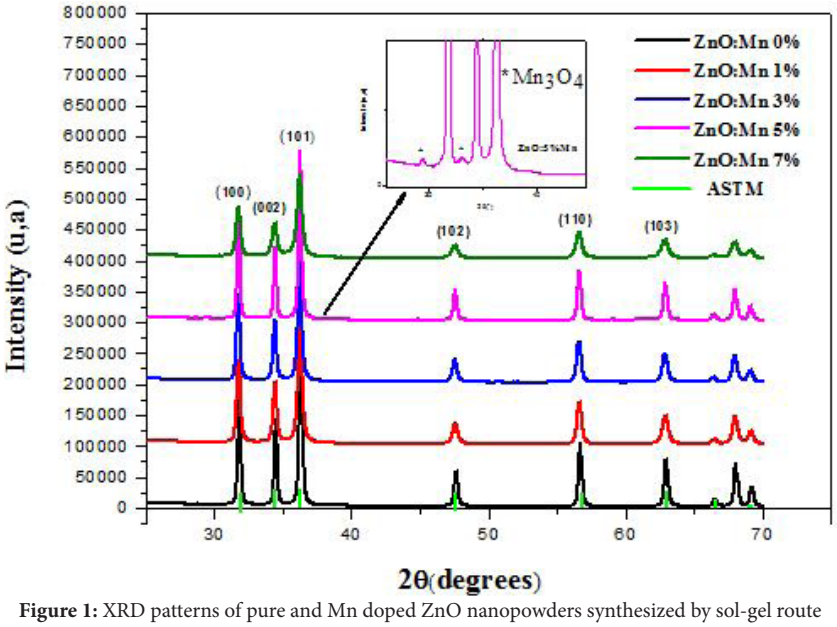

Figure 1: XRD patterns of pure and Mn doped ZnO nanopowders synthesized by sol-gel route

As it is shown in Figure 3 the grain size of Mn doped ZnO nanopowders decreases by increasing Mn concentration and varies from 65.92 nm to 36.15 nm, except for 5% mol Mn, where there is an unexpected increase, the grain size becomes higher (D ≈ 66 nm) because of the appearance of the new phase Mn_3O_4. However the powders keep the same structure. The values of lattice parameters are listed in Table 1.

The diffraction peaks of the ZnO matrix are slightly shifted towards the small angles after introduction of Mn atoms. It indicates that Mn^{2+} ions go to Zn^{2+} sites. The ionic radius of Zn^{2+} being 0.60 A°, and the one of Mn^{2+} is 0.66 A°.

Zn% MnO	a=b(A°)	c(A°)	c/a	D (XRD) (nm)	D (TEM) (nm)
0% mol Mn	3.2425	5.2012	1,6037	65.92	59.86
1% mol Mn	3.2432	5.2064	1.6053	52.51	55.39
3% mol Mn	3.2565	5.2025	1.6000	47.47	42.13
5% mol Mn	3.2458	5.1953	1.5975	66.97	65.12
7% mol Mn	3.246	5.2021	1.6022	36.15	39.40

Table1: The lattice parameters, crystalline size and particle size of Mn doped ZnO samples synthesized by sol-gel route

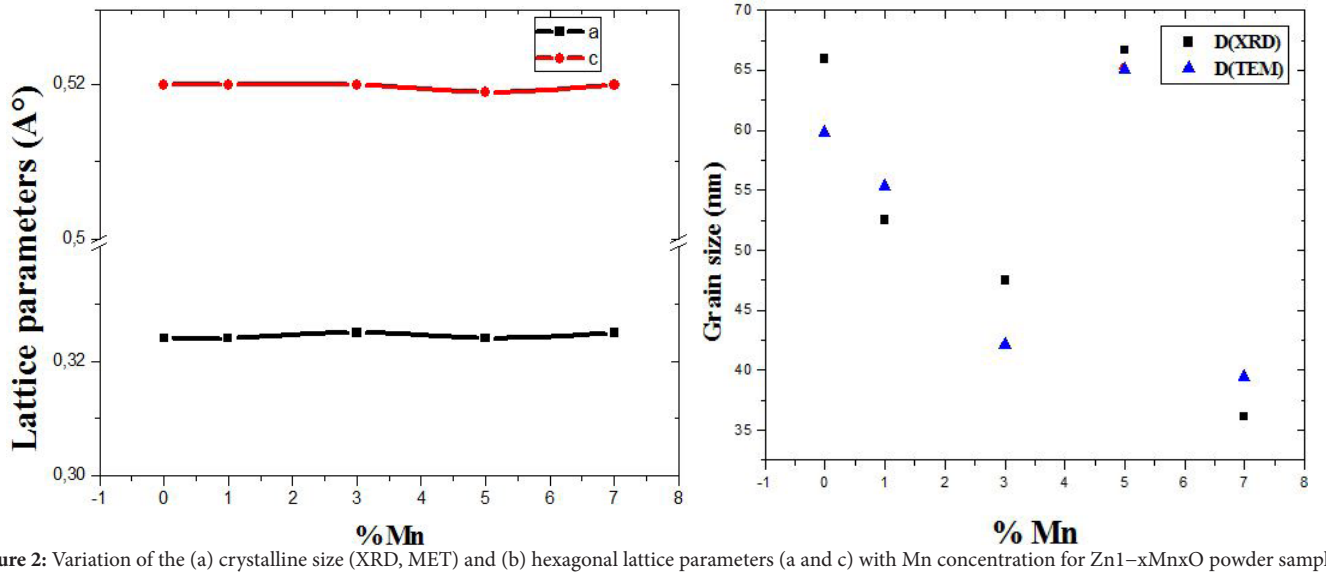

Figure 2: Variation of the (a) crystalline size (XRD, MET) and (b) hexagonal lattice parameters (a and c) with Mn concentration for Zn1−xMnxO powder samples

In Figure 4, we present TEM images of the pure ZnO and manganese-doped ZnO nanopowders. The images show that the crystallites tend to agglomerate and form aggregating sphere. This tendency has already been reported by Phoka, *et al.* [22]. Basically, nanoparticles have a natural trend to agglomerate for two main reasons. First, the agglomeration is a more stable configuration from an energetic point of view. Then, nanoparticles tend to agglomerate to allow crystallite growth.

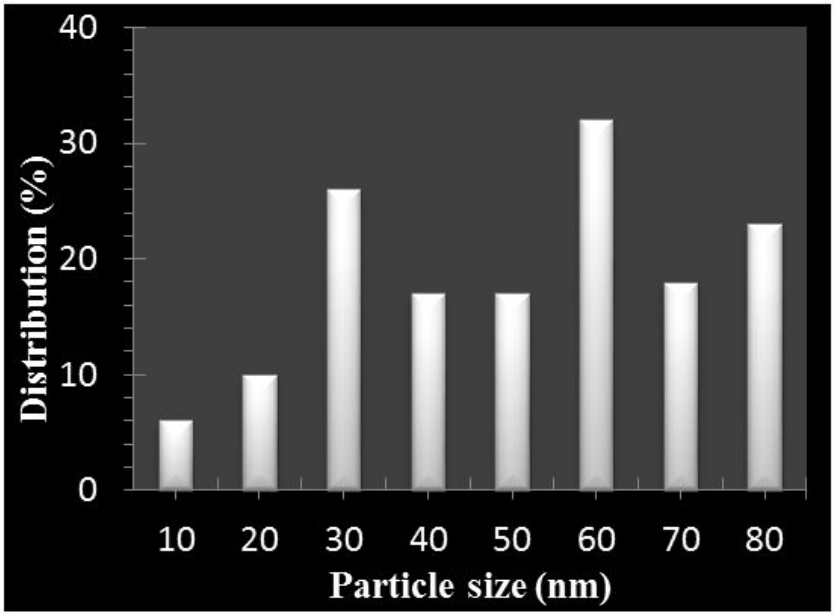

Figure 3: Average distribution of particle size of pure and Mn doped nanopowders

The results presented in Figure 3 indicate that the mean crystallite sizes measured from the TEM images is varying in the same direction than those obtained by XRD. The crystallite size histograms of pure ZnO, 1 mol%, 3 mol%, 5 mol% and 7 mol% manganese-doped nanoparticles are shown in Figure 3. For the doped samples, the crystallite size is between 10 and 80 nm. The manganese doping causes a reduction in the number of crystallites belonging to the size range from 39.4 to 79.87 nm.

However, the sample doped with 5 mol% Mn contains the Mn_3O_4 phase, whose crystallite size is on average higher than those obtained with the other concentrations. Since it is not possible to distinguish the mechanism of agglomeration of ZnO crystallites from Mn_3O_4 crystallites on a TEM image, we suggest that our measurements involve crystallites of the Mn_3O_4 phase because of the larger size of these crystallites.

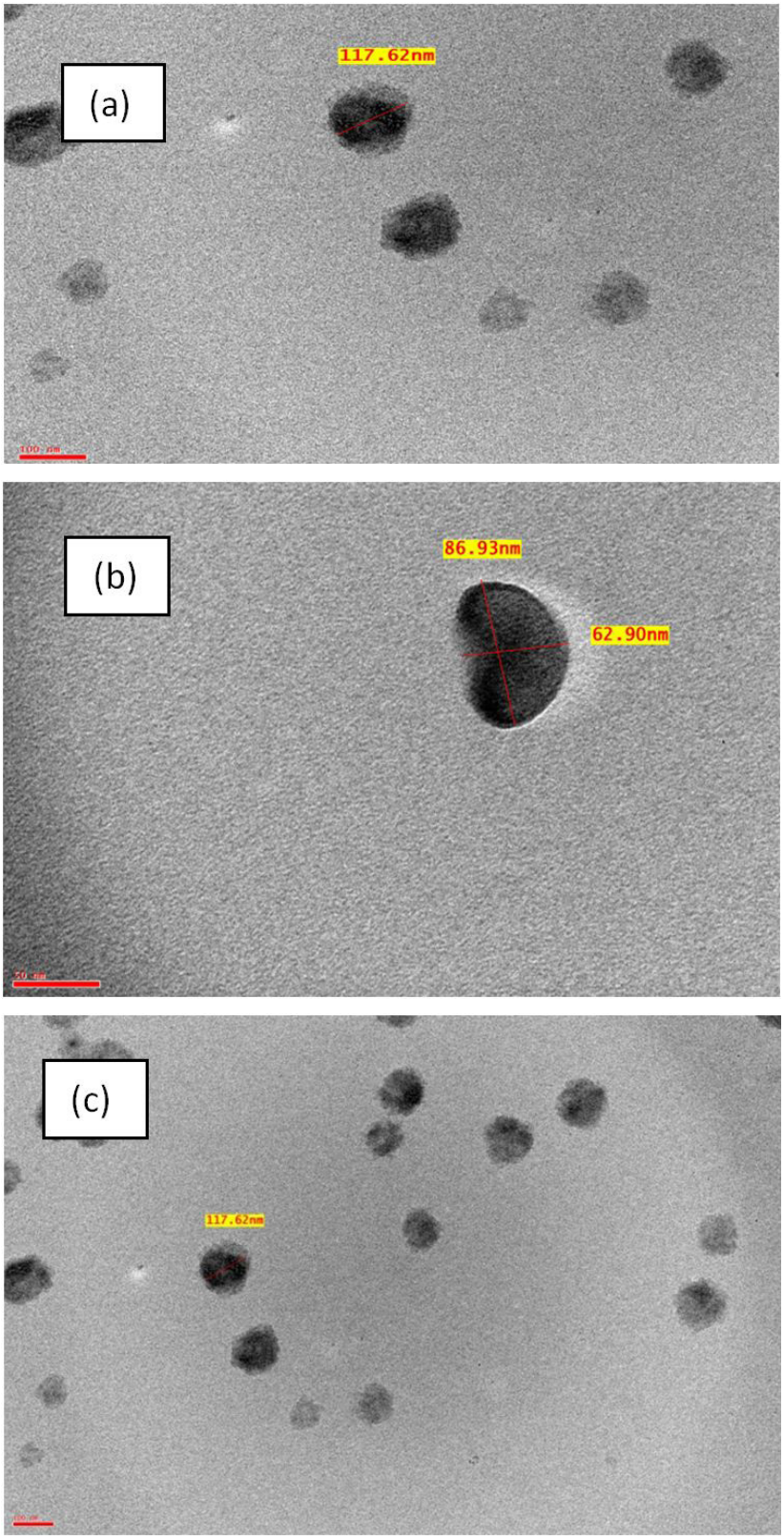

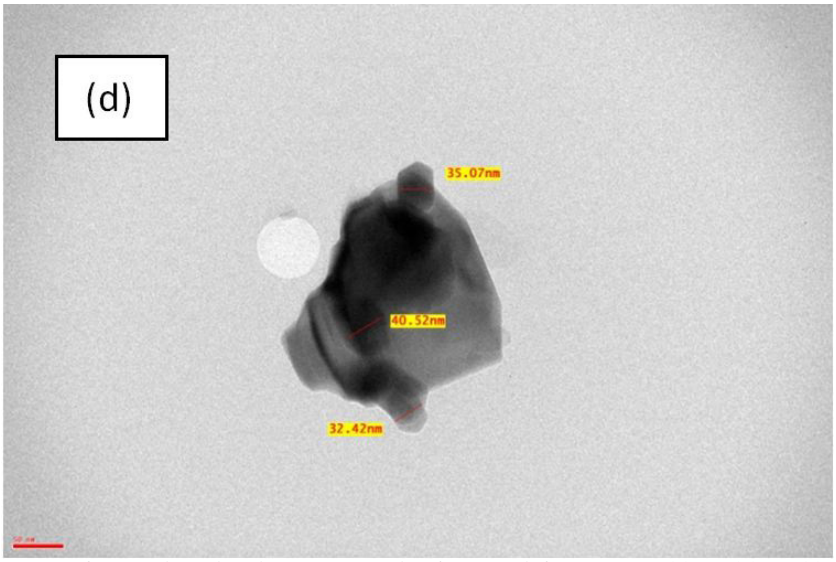

Figure 4: TEM images of pure and Mn doped ZnO nanopowders from two different regions. (**a**) 0%, (**b**) 1%, (**c**) 3%, and (**d**) 5%

The plotted electric field as a function of current density for different concentrations is given in Figure 6. The nonlinear coefficient α was obtained by: α=log (I2/I1)/ (V2/V1) where V1 and I1 as well as V2 and I2 are corresponding values of voltage and current for two points that can be chosen arbitrarily in the non-ohmic region [23].

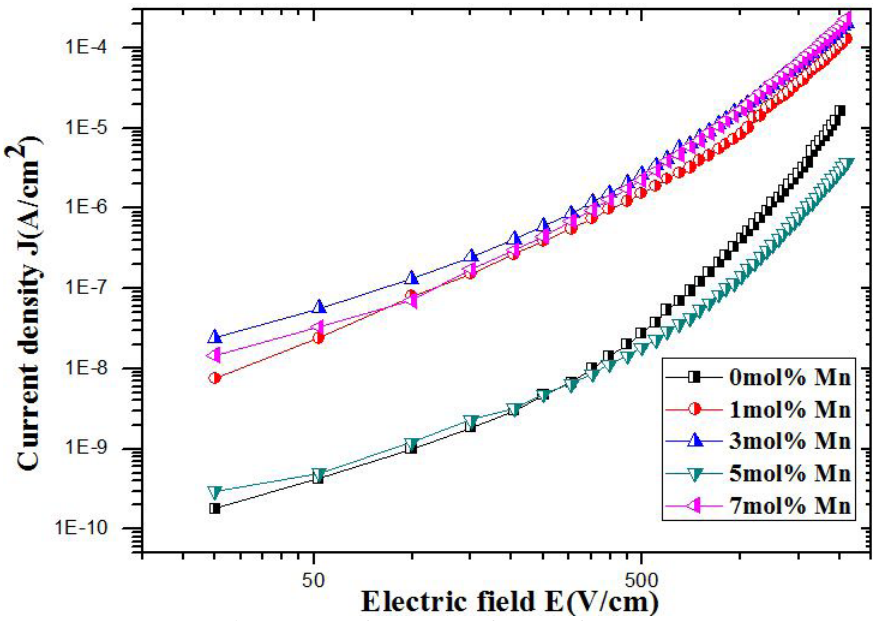

Figure 5: Characteristics of varistors as a function of Mn concentration

E(J) curves obtained at room temperature for all the samples are shown in Figure 5. We can see clearly two regions: the ohmic region, known as a high resistance region and the non-ohmic one, known as a very low resistance region.

The curves show that the electric field E in the non-linear region increases by increasing Mn concentration, thus E increases with decreasing of grain and particle sizes except for 5 mol% Mn, where E is lower and the grain size higher. However the current density is reduced, particularly for the 5 mol% Mn, because the current is limited to the ohmic resistance. This is in good agreement with XRD and TEM results, and can be explained by the increase of the number of grain boundaries due to the decrease of the grain size average.

Table 2 and Figure 6 show that the non-linear coefficient and the breakdown voltage increase by increasing Mn concentration up to 3mol % Mn and remain nearly constant after that. The Zn-5%Mn-O is still out the expect variation.

For the coefficient α the results can be explained by the fact that this coefficient is due to solid state reactions and the formation of potential barriers between grains [24].

The increase of EB with increasing Mn concentration (from 1595V/cm to 1901.50V/cm except for the Zn-5%Mn-O varistor) and by the fact its increase with decreasing of the grain size of starting powders can be explained by the increase of the number of grain boundaries due to the decrease of the grain size average.

Sample	Breakdown voltage (V/cm)	Non-linearity coefficient α
0% mol Mn	1595	2.8450
1% mol Mn	1659.88	3.7973
3% mol Mn	1851.32	3.63
5% mol Mn	1773.33	3.40
7% mol Mn	1901.50	13.63

Table 2: The varistor effect parameters of pure and Mn doped ZnO samples synthesized by sol-gel route

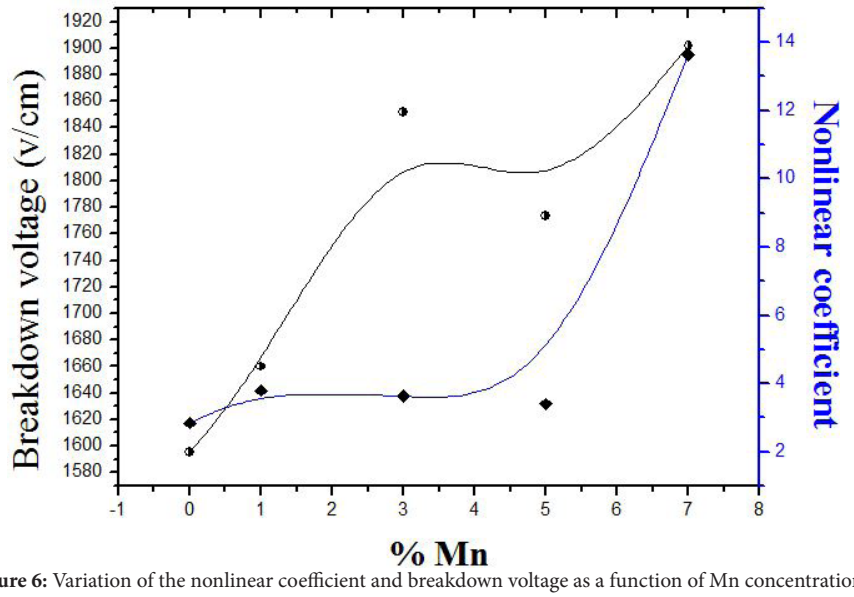

Figure 6: Variation of the nonlinear coefficient and breakdown voltage as a function of Mn concentration

Conclusion

Nanopowders of pure and Mn (1–7%) doped ZnO have been synthesized by Sol–gel technique. The obtained nanopowders have been characterized by means of XRD, TEM and I-V to determine, respectively, their structural characteristics, morphological and electrical properties. The all obtained powders exhibit würtzite structure, where the lattice parameters a and c vary in the same direction. These powders are constituted by very small grains, which size decreases as a function of Mn concentration. On the other hand the manganese doping causes a decrease in the particles size and an increase in varistor effect for the 1, 3 and 7 mol% Mn-doped samples; the breakdown electric field ranges between 1595/cm and 1901.50V/cm except and the coefficient of non-linearity (α) between 2.8450 and 13.63. In comparison with previous researches we have recorded higher values of non-linearity coefficient [25].

All samples have a morphology consisting of small nanoparticles, uniformly distributed. From 5 mol% Mn and more, the powders contain a Mn3O4 secondary phase formed at grain boundaries, which is not suitable for a use as varistor. This study shows that 7 mol% Mn doped ZnO varistor has the best electrical properties.

References

1. Wang X, Song J, Wang Z.L (2007) Nanowire and nanobelt arrays of zinc oxide from synthesis to properties and to novel devices. J Mater Chem. 17: 711-20.

2. Matsuoka M, Masuyama T, Iida Y (1969) Voltage nonlinearity of zinc oxide ceramics doped with alkali-earth metal oxide. Jap J Appl Phys. 81275–6.

3. Subasri R, Asha M, Hembram K, Rao GVN, Rao TN (2009) Microwave sintering of doped nanocrystalline ZnO and characterization for varistor applications. J Mat Chem Phy. 115: 677-84.

4. Levinson LM, Philipp HR (1975) The physics of metal oxide varistors. J Appl Phys 46: 1332-4.

5. Clarke DR (2004) Varistor ceramics. J Am Ceram Soc. 82: 485-502.

6. Pianaro SA, Bueno PR, Longo E, Varela JA (2009) Comparison of non-Ohmic accelerated ageing of the ZnO- and SnO_2-based voltage dependent resistors. J Phy Appl Phy 14: 692.

7. S.Bernik, N Daneu, A Rečnik (2004) Inversion boundary induced grain growth in TiO_2 or Sb_2O_3doped ZnO-based varistor ceramics. J Euro Ceram Soc 24: 3703-8.

8. Wen-Bin S, Jin-Feng W, Hong-Cun C, Wen-Xin W, Guo-Zhong Z, et al. (2002) Nonlinear electrical behavior of the TiO_2.WO_3 varistor. J Appl Phy 92: 4779.

9. Daniel GS, Tania Regina GO, Edson RL, José AV, Elson L (2008) Nanostructured TiO_2 thin films by polymeric precursor method. Chem New 31: 79.

10. Kosuke T, Wei-Ting C, Hanzheng G, Wen-Hsi L, Sophie GF, et al. (2017) Contrasting conduction mechanisms of two internal barrier layer capacitors: (Mn, Nb)-doped $SrTiO_3$ and $CaCu_3Ti_4O_{12}$. J Appl Phy 121: 064107.

11. MS Castro, CM Aldao (1998) Prebreakdown conduction in zinc oxide varistors: Thermionic or tunnel currents and one step or two step conduction processes. J Appl Phy 63: 1077.

12. Daisuke N, Hiroshi F, Kazuo S, Nobuyasu M (1998) Electrical properties of semiconductive Nb-doped BaTiO3 thin films prepared by metal–organic chemical-vapor deposition. A Appl Phy 72: 2017.

13. Yang XS, Wang Y, Dong L (2004) WO_3-based capacitor–varistor doped with Gd_2O_3. Mater Chem Phys 86: 253–257.

14. CP Li, JF Wang, WB Su, HC Chen, WX Wang, et al. (2001) Nonlinear electrical properties of cobalt doped SnO_2,•Ni_2O_3,•Nb_2O_5 varistors. Eur Phys J 16: 3-9.

15. Tetsuya S, Richard CB (1990) Grain growth in sintering ZnO and ZnO–Bi_2O_3 ceramics. J Am Ceram Soc 75: 2529-34.

16. Nahm CW (2003) nonlinear properties and stability against DC accelerated aging of praseodymium oxide-based ZnO varistors by Er_2O_3 doping. Solid State Commun. 126: 281-4.

17. Hashimov AM, Hasanli SM, Mehtizadeh RN, Bayramov KB, Azizoya SM (2006) Zinc oxide and polymer-based composite varistors. Phys Stat Sol 3: 2871-5.

18. Blatter G, Greuter F (1986) Carrier transport through grain boundaries in semi-conductors. Phys Rev B 33: 3952–66.

19. Sharma VK, Varma GD (2008) Investigations of the effect of gaseous environment during synthesis on the magnetic properties of Mn doped ZnO. J Alloys Compounds. 458: 523-7.

20. Jin ZC, Hamberg J, Granqvist CG (1988) Optical properties of sputter-deposition ZnO:Al thin films. J Appl Phys 64: 5117.

21. Liu HY, Kong H, Ma XM, Shi WZ (2007) Microstructure and electrical properties of ZnO-based varistors prepared by high-energy ball milling. J Mat Sci 42: 2637-42.

22. Gupta TK (1990) Application of zinc-oxide varistors. J Am Ceram Soc 73: 1817-40.

23. Duran P, Tartaj J, Moure C (2003) Fully dense, fine-grained, doped zinc oxide varistors with improved nonlinear properties by thermal processing optimization. J Am Ceram Soc 86: 1326-9.

24. Mirzayi M, Hekmatshoar MH (2013) Effect of V_2O_5 on electrical and microstructural properties of ZnO ceramics. Phys B 414: 50-5.

25. Michio M (1970) Nonohmic Properties of Zinc Oxide Ceramics. Japan Soc Appl Phy 10: 10-6.